LIP-STUDENTS-25-14

Cosmic Materials: Data & Simulation in Action

Isabel Dias[1,a]

[1] *Instituto Superior Técnico, Lisboa, Portugal*

Project supervisor: Bruna Lima

September 30, 2025

Abstract. This report describes the work developed in the framework of an internship focused on cosmic radiation analysis. Simulations and experimental data were used to study radiation interactions with different materials for GCR's under minimum and maximum solar periods and for the SEP event of September 2017. The environments studied were the Earth, the Moon, Mars and Interplanetary Space. The goal was to analyze key variables such as energy and angular distributions and Linear Energy Transfer (LET). The work combines hands-on analysis with ROOT of the dMEREM simulation encoded in the PlanetRAD setup.

Keywords: Space radiation, Galactic Cosmic Rays, Solar Energetic Particles, LET (Linear Energy Transfer), dMEREM, PlanetRAD, Earth, Mars, Moon, radiation dose.

1 Introduction

During this internship, the goal was to understand space radiation environments and the effects of the interactions of high-energy particles with different materials. This is a crucial aspect of space exploration, as radiation affects both humans and spacecraft. Long-term exposure, particularly to high-LET particles, can cause severe damage to DNA in living cells and degrade the performance of electronic systems. Therefore, accurately simulating radiation effect is essential for mission planning, suppoting the development of protective shielding and operational strategies that ensure mission safety.

In this context, experimental measurements and Monte Carlo simulations are complementary tools for characterizing radiation interactions with shielding materials and biological matter. Experimental data provides direct information on dose distributions and particle behavior under controlled conditions, while simulations make it possible to explore a wider range of energies, geometries, and space environments that are impractical to reproduce in the laboratory and to measure directly in situ. By combining both approaches, we can obtain a more reliable understanding of the space radiation environment and more effectively evaluate potential countermeasures for future missions.

In this work, both ROOT histograms and Geant4-based simulations were analyzed to investigate energy distributions, linear energy transfer (LET), and particle fluxes in different materials, with the goal of comparing simulation outputs against physical expectations.

2 General Physics of Radiation

Radiation is broadly defined as the emission and propagation of energy in the form of electromagnetic waves or energetic particles. A distinction can be made between *non-ionising radiation*, such as radio waves, visible light, or microwaves, and *ionising radiation*, which carries sufficient energy to remove electrons from atoms and molecules. In the context of space environments, the most relevant component is ionising radiation, primarily composed of protons, α-particles, heavy ions, electrons, and secondary neutrons and photons generated in matter interactions.

When energetic charged particles traverse matter, they lose energy mainly through excitation and ionisation of the atoms in the medium. This process is continuous and well described by the Bethe–Bloch equation, which expresses the mean rate of energy loss per unit path length, also known as the stopping power:

$$-\left\langle \frac{dE}{dx} \right\rangle = \frac{4\pi}{m_e c^2} \cdot \frac{nz^2}{\beta^2} \cdot \left(\frac{e^2}{4\pi\varepsilon_0} \right)^2 \cdot \left[\ln\left(\frac{2m_e c^2 \beta^2}{I \cdot (1-\beta^2)} \right) - \beta^2 \right] \tag{1}$$

where:

- $\frac{dE}{dx}$ is the mean energy loss per unit path length (stopping power),
- m_e is the electron mass,
- c is the speed of light,
- n is the electron density of the medium,
- z is the charge of the incident particle in units of the elementary charge,
- $\beta = v/c$ is the particle's velocity relative to the speed of light,
- e is the elementary charge,
- ε_0 is the vacuum permittivity,
- I is the mean excitation potential of the absorber material.

This fundamental equation underpins the concept of *Linear Energy Transfer* (LET), defined as the energy deposited by radiation per unit length of its track in matter. Radiation with a high LET, such as heavy ions and α-particles, deposits large amounts of energy locally, causing severe biological and material damage. Conversely, low LET radiation, such as electrons or high-energy protons, deposits energy more sparsely, resulting in a different risk profile.

[a] e-mail: isabel.noronha.dias@tecnico.ulisboa.pt

3 Space Radiation Environment

3.1 Galactic Cosmic Rays (GCRs)

The most significant component of the cosmic ray spectrum is Galactic Cosmic Radiation (GCR), which is a continuous source of ionising radiation with origin outside the Solar System. They are dominated by protons ($\approx$ 87%), followed by α-particles ($\approx$ 12%) and a smaller fraction of fully ionised heavy nuclei ($\approx$ 1%) up to iron [1].

Their energies span from below 1 MeV/nucleon up to about 10^{21} eV, although the most hazardous biological and technological effects are associated with nuclei in the range of 100 MeV/nucleon to a few GeV/nucleon, due to its flux characteristics. The GCR spectrum approximately follows a power-law distribution above the GeV/nucleon scale, with a broad maximum around a few GeV/nucleon. Because of their high penetration power, GCR's affect spacecraft systems and astronaut health.

Figure 1 illustrates the cosmic ray intensity spectrum, following an approximate power-law behavior $I(E) \sim E^{-2.7...3.0}$ [2], which reflects the different sources contributing to GCR's.

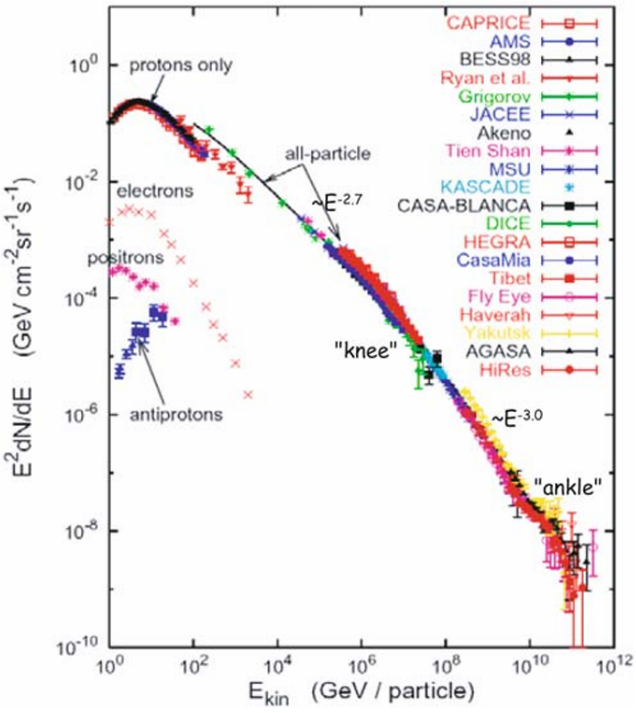

Figure 1: Cosmic ray intensity spectrum, spanning more than ten orders of magnitude. Taken from [2].

3.2 Solar Energetic Particles (SEPs)

Superimposed on the continuous GCR background are sporadic Solar Energetic Particle (SEP) events. SEPs consist mainly of protons and electrons, with contributions from helium nuclei ($\approx$ 10%) and heavier ions ($<$ 1%). Their energies range from a few keV up to $\sim$ 1 GeV/nucleon, generally lower than those of GCRs, but their intensities can increase abruptly during solar activity.

SEPs are produced by two main mechanisms:

- **Impulsive events**, associated with solar flares, are short-lived (lasting hours), rich in heavy ions, but relatively poor in protons.
- **Gradual events**, associated with coronal mass ejections (CMEs), are longer (lasting days), proton-dominated, and spread over large heliospheric regions.

These events are central to space weather studies, as they can significantly increase radiation exposure during interplanetary missions. Their stochastic nature, in terms of frequency, duration, and spectral intensity, makes them a major concern for astronaut safety, particularly during extravehicular activities (EVA) with limited shielding.

3.3 Planetary Radiation Belts

Planets with magnetic fields, such as Earth, Jupiter, and Saturn, host radiation belts formed by energetic charged particles trapped along magnetic field lines.

Radiation belts are important not only on Earth, but also for any mission that requires crossing this environment. Additionally, these represent an important factor to take into consideration in other planets such as Jupiter, where intense trapped particle populations pose a major challenge to spacecraft. Recent missions, such as ESA's JUICE spacecraft, carry dedicated instruments like the Radiation hard Electron Monitor (RADEM) [3] —developed with contributions from LIP and the SpaceRad research group—to study trapped radiation environments.

3.4 The Solar Cycle

The Sun exhibits an approximately 11-year cycle of magnetic activity, commonly referred to as the solar cycle. This cycle is characterised by the rise and fall in the number and total area of sunspots, which serve as indicators of solar activity.

During solar maximum, sunspot numbers peak, and the probability of the ocurrence of solar flares and coronal mass ejections increases, producing more frequent and intense SEP events. At the same time, the enhanced solar magnetic field and solar wind provide greater shielding against GCRs, leading to a significant reduction in their flux. Conversely, during solar minimum, SEP activity is low, but the reduced solar magnetic shielding allows GCRs to penetrate more easily into the inner solar system, resulting in a higher GCR flux.

The difficult balance between more sporadic and dangerous events, but simultaneously less base GCR implications add to the complexity of the problem, and affect mission planning very directly.

4 Simulation Setup

4.1 dMEREM

The detailed Mars Energetic Radiation Environment Model (dMEREM) serves as the foundation of this project.

dMEREM was developed and validated by the SpaceRad research group at LIP [4] [5]. It is a Geant4-based Monte Carlo simulation toolkit, implemented in C++ and C, with ROOT libraries used for analysis [6]. Its main purpose is to study the Martian radiation environment by simulating the interactions of Galactic Cosmic Rays (GCRs), Solar Energetic Particles (SEPs), and secondary albedo particles with the soil and atmosphere of Mars.

dMEREM is integrated into the SPENVIS platform, available on http://www.spenvis.oma.be/intro.php, which provides user-friendly access to the scientific community. Researchers can define accurate inputs, execute Monte Carlo simulations, and analyze outputs through SPENVIS, making dMEREM a powerful mission-planning tool for Mars exploration. Published studies (see [4] and [5]) validate the accuracy of dMEREM, particularly in the context of landing site analyses, demonstrating its usefulness for radiation environment characterization .

4.1.1 Geant4

Geant4 (**GE**ometry **AN**d **T**racking) is the backbone of dMEREM. It is a widely used Monte Carlo simulation toolkit designed to model the passage of particles through matter. Geant4 provides extensive functionality, including particle tracking, complex geometry handling, and physics processes that cover electromagnetic, hadronic, and optical interactions over a broad energy range, from sub-keV to the TeV scale.

The toolkit is developed collaboratively by physicists and software engineers and is implemented in C++, using object-oriented programming principles. It is employed in particle physics, nuclear physics, accelerator design, space applications, and medical physics. In the context of dMEREM, Geant4 enables the simulation of primary and secondary particles—including electrons, protons, neutrons, and heavy ions—interacting with Mars' atmosphere and surface. Through random sampling, it models the stochastic nature of particle transport and energy deposition, yielding physical quantities essential for radiation studies.

4.1.2 Functionalities of dMEREM

To accurately model Mars' environment, dMEREM incorporates several environmental and physical parameters. It uses a 20-layer atmosphere extending up to 50 km and simulates 100 m of soil over a horizontal span of 300 km. When magnetic fields are included, the atmosphere is extended by an additional 100 km, and the soil width by 900 km.

Radiation inputs can be defined to represent either GCRs or SEPs by selecting the particle types, energy ranges, and number of primaries. After simulation, the output is stored in a ROOT file containing key variables for each particle, such as energy and angle. Analysis scripts then process this raw output into physical observables, such as flux spectra, which are later interpreted in the results section.

4.2 PlanetRAD

PlanetRAD was developed as a visualization and companion tool for dMEREM, providing users with an intuitive graphical interface to configure and run simulations. While dMEREM was originally validated only for the Martian surface, PlanetRAD extends its applicability by generalizing the framework to a wider range of environments, including:

- Earth's surface (using standard atmosphere),
- Mars (Gale Crater),
- Moon (regolith),
- Interplanetary space.

The selectable spectra are:

- GCR (solar minimum),
- GCR (solar maximum),
- SEP (September 2017 event).

Additionally, users may choose fixed mono-energetic sources (e.g., α, proton, gamma, electron, or geantino), define their energy, and set the number of primaries. A run ID can be assigned to facilitate tracking of multiple simulations.

PlanetRAD also includes a visualization mode, allowing users to observe the simulated environment and particle trajectories. However, this feature is practical only for small numbers of primaries due to computational cost (see Appendix 14 for example).

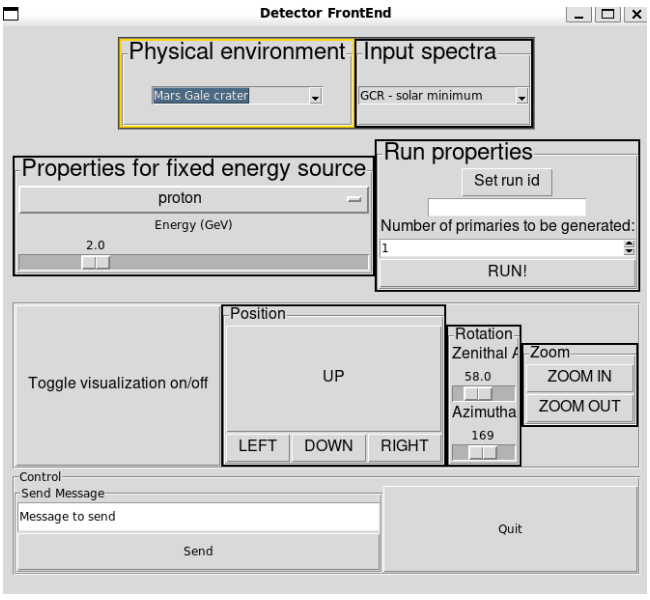

Figure 2: PlanetRAD graphical user interface. Users can select the environment, radiation spectra or fixed particle source, number of primaries, and run configuration for the simulation.

4.3 Outputs

The simulation outputs are stored as ROOT files containing histograms of relevant observables, including:

- `ChargedTheta`, `ElecTheta`, `GammTheta`,
- `NeutEnergy`, `NeutTheta`,
- `PrimEnergy`, `PrimCosTheta`, `PrimTheta`,
- `ProtCosTheta`, `ProtEnergy`, `ProtTheta`.

These histograms are typically expressed in counts versus variable (e.g., counts vs. energy). A crucial step in the analysis, presented in the next section, is the conversion of raw counts into differential flux, thereby enabling meaningful physical interpretation of the simulation results.

4.4 Normalization Factor

After each run, PlanetRAD produces a summary text output with relevant simulation parameters. An excerpt is shown below:

```
Run Summary
  Number of events processed : 50000
  ...
  dMEREMRunAction: dOmegaGen 2.70827
  dMEREMRunAction: fNorm 1.48757e-16
  dMEREMRunAction: Event normalisation factor
  1.48757e-05
  fNormU 1.48757e-05
```

Among these quantities, the most important is the *Event normalization factor*, f_{NormU}. From the `dMEREMRunAction.cc` implementation, the normalization is computed as:

$$f_{\mathrm{Norm}} = \frac{\Phi_{\mathrm{primary}}}{N_{\mathrm{gen}}/\Delta\Omega_{\mathrm{gen}}}, \tag{2}$$

where Φ_{primary} is the primary flux (particles/cm^2/sr/s), N_{gen} is the total number of generated events, and $\Delta\Omega_{\mathrm{gen}}$ is the solid angle sampled in the simulation.

The unit-normalized factor is then given by

$$f_{\mathrm{NormU}} = \frac{f_{\mathrm{Norm}}}{U_{\mathrm{flux}}}, \tag{3}$$

with U_{flux} being the flux unit (typically 10^{-11}/cm^2/MeV/sr/s in PlanetRAD).

To convert histogram counts into a differential flux, the relation is:

$$\frac{d\Phi}{dE} = \frac{N_{\mathrm{counts}} \cdot f_{\mathrm{NormU}}}{\Delta E}, \tag{4}$$

where N_{counts} is the number of entries in a bin, ΔE is the bin width in energy, and $d\Phi/dE$ is expressed in units of particles/(cm^2 sr s MeV).

Thus, the conversion from counts to flux involves multiplying the raw counts by the normalization factor and dividing by the bin width. This ensures that the spectra obtained from PlanetRAD are directly comparable to experimental data and other radiation environment models.

4.5 Simulation Parameters

To compare radiation environments and particle transport under different planetary and interplanetary conditions, a total of 12 simulations were performed. These correspond to the combination of three input spectra—Galactic Cosmic Rays at solar minimum, Galactic Cosmic Rays at solar maximum, and the September 2017 Solar Energetic Particle event—with four environments: Earth's atmosphere, Mars' Gale Crater, the Moon's regolith, and interplanetary space. The simulations were carried out using PlanetRAD/dMEREM with **50,000** primary particles per run.

The statistical uncertainties for each histogram were calculated based on the number of counts per bin, following Poisson statistics. In bins with a low number of counts, such as those observed in Earth's atmosphere simulations, the relative uncertainties are larger, while in environments with higher fluxes, like the Moon or interplanetary space, uncertainties are comparatively smaller. These uncertainties are reflected in the error bars shown in the figures and provide an estimate of the confidence in the simulated fluxes and derived quantities.

5 Simulation Results and Analysis

5.1 Interplanetary Space

In interplanetary space, with no shielding from planetary magnetospheres or atmospheres, the detector is directly exposed to the full spectrum of cosmic radiation. This environment serves as a reference for comparison with planetary cases, as it represents the unattenuated background flux.

In Figure 3, the GCR flux is shown for both solar minimum and solar maximum. As expected, the flux is higher during solar minimum, due to the reduced shielding effect of the solar magnetic field and solar wind modulation. This trend will also be observed in the other environments.

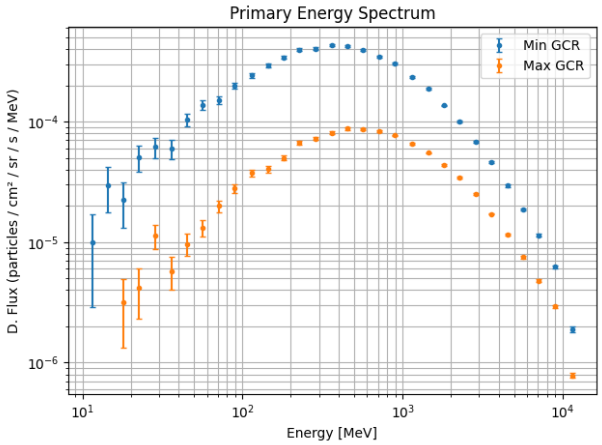

Figure 3: Galactic Cosmic Ray flux in interplanetary space for solar minimum and maximum conditions.

In Figure 4, the Solar Energetic Particle (SEP) flux from the September 2017 event is displayed. SEPs can

temporarily dominate the radiation environment, reaching flux levels significantly higher than GCRs, but lower in energy, as explained in the introduction 3.2.

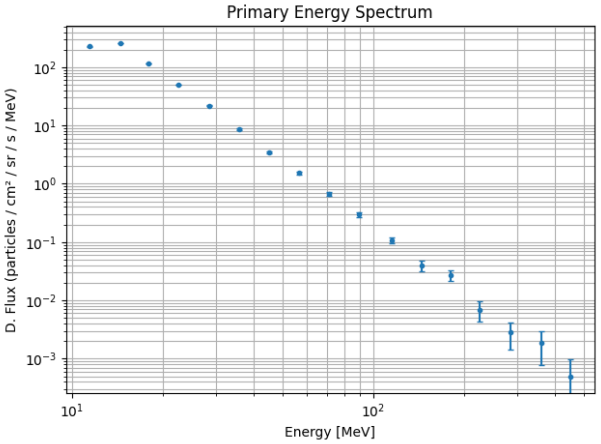

Figure 4: Solar Energetic Particle Proton flux in interplanetary space (September 2017 event).

This unshielded case provides the baseline for evaluating how planetary environments, such as Earth's atmosphere, modify the incoming radiation spectrum.

5.2 Earth Atmosphere

The radiation environment at the Earth's surface is strongly shaped by two protective layers: the magnetosphere and the atmosphere.

In our simulation results, this shielding effect is clearly visible. Out of the 50,000 proton primaries generated, only 52 were detected at the surface, a dramatic reduction compared to the unshielded interplanetary case. This steep drop in statistics is reflected in the larger uncertainties of the spectrum, which stand out relative to the other environments studied 5. The particles that do reach the surface are restricted to the highest energies, capable of traversing the atmosphere with minimal attenuation. Lower-energy primaries are almost entirely absorbed, undergoing strong energy loss and producing secondary cascades that remain confined within the atmosphere.

This strong attenuation highlights the efficiency of Earth's natural shielding and provides a useful contrast with less protected environments, such as the Martian surface.

5.3 Mars Gale Crater

In contrast to Earth, Mars lacks a global magnetic field and is only partially shielded by weak crustal magnetic anomalies. Its atmosphere is also extremely thin, with column depths of 15–22 g/cm² at the surface, which is 50–70 times lower than the 1,030 g/cm² average at Earth's sea level. This reduced shielding allows a far greater fraction of Galactic Cosmic Rays (GCRs) and Solar Energetic Particles (SEPs) to penetrate the Martian environment. As

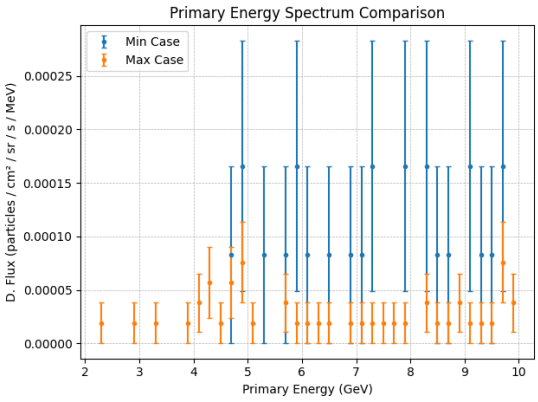

Figure 5: GCR proton particle flux entering Earth's atmosphere for solar minimum and maximum conditions.

a result, the radiation field at the Martian surface is both more intense and compositionally different from that on Earth.

High-energy GCRs interact with the sparse atmosphere and the regolith, producing secondary particle showers. Protons above 150 MeV can reach the surface directly, where they undergo spallation and fragmentation processes that generate albedo neutrons and energetic gamma rays, further contributing to the local radiation environment.

In Figure 6 the angular distribution of secondary gamma flux at the Martian surface is presented. The relatively thick appearance of the curve indicates a large number of recorded events, consistent with the high flux of secondary radiation generated by primary GCR interactions with the thin atmosphere and regolith. This demonstrates that not only do many particles reach the surface, but their interactions also give rise to a significant population of secondary gammas that contribute to the radiation environment.

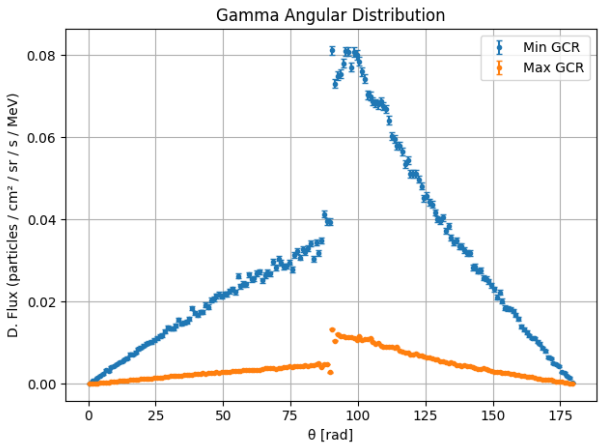

Figure 6: Angular distribution and flux of secondary gamma rays at the Martian surface, highlighting their production through interactions of GCRs with the atmosphere and regolith.

It's important to note that in the angular distributions of secondary particles, a visible discontinuity appears at $\theta = 90°$. The angle θ is measured with respect to the incoming primary particle direction, such that $\theta < 90°$ corresponds to forward-going particles (propagating deeper into the medium) and $\theta > 90°$ corresponds to backward-going particles (escaping upward). When both forward- and backward-directed particles are present, the histogram separates the two hemispheres at exactly $\theta = 90°$, introducing an artificial gap at that boundary.

This effect is systematic across the particle species discussed in this report, whenever contributions are recorded from both sides of the medium. The overall asymmetry between forward and backward hemispheres is physically meaningful: for Mars, there are more gammas in the backward hemisphere, as the ones coming forward are more attenuated by the atmosphere. This also reflects on the fact that particles hitting downward tend to follow the distribution of the generated primaries, which is head on, while the ones going away can take on a more wide range of angles.

Figure 7 compares the GCR fluxes at solar minimum and maximum for Mars. The solar minimum case is very similar to the unshielded interplanetary spectrum, while the solar maximum case shows attenuation by the atmosphere. However, even in the maximum case, the flux at the Martian surface remains much higher than on Earth, with a significantly larger number of primaries reaching the detector (95.4%).

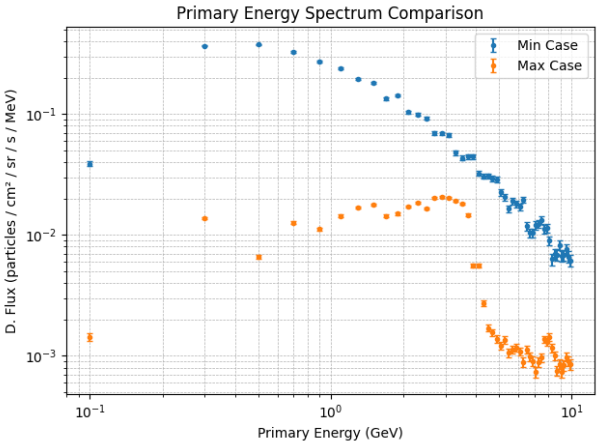

Figure 7: GCR proton particle flux reaching the surface of Mars' Gale Crater for solar minimum and maximum conditions.

These results highlight the importance of secondary radiation on Mars, particularly gammas produced through spallation and fragmentation. This trend will also be observed in the following section, where we analyze the Moon case, in which the absence of an atmosphere emphasizes the role of secondary particles, especially neutron production, in shaping the local radiation environment.

5.4 Moon Regolith

The lunar radiation environment is shaped by the absence of both a global magnetic field and a protective atmosphere, leaving the surface fully exposed to Galactic Cosmic Rays (GCRs), Solar Energetic Particles (SEPs), and solar UV/X-rays. These interact with the regolith, producing secondary radiation (notably neutrons, protons, and gammas), and cause physical and chemical modifications such as dielectric breakdown, changes in porosity, and measurable variations in albedo.

From a radiation perspective, the Moon is particularly interesting: it experiences the full primary fluxes of GCRs and SEPs while also producing substantial albedo secondaries that directly impact dose rates, that have meaningful impacts on space exploration and lunar surface operations.

In Figure 8, we compare the GCR spectra at solar minimum and maximum with the interplanetary reference. The lunar environment shows minimal attenuation: almost all primaries simulated reach the detector (99.9%), in contrast to the strong shielding effects observed for Earth. This reinforces that the Moon, like interplanetary space, provides essentially no natural protection against the incident radiation field.

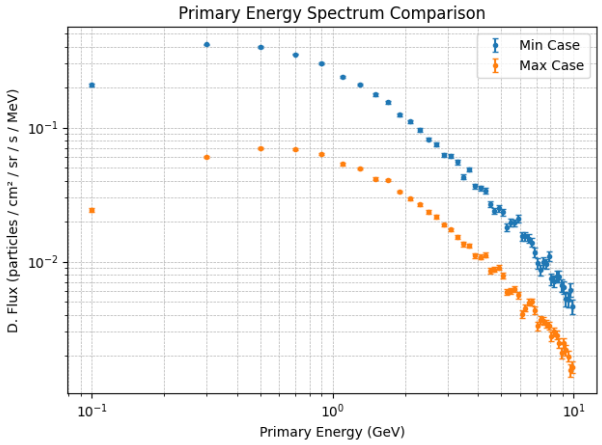

Figure 8: GCR proton particle flux reaching the surface of Moon's regolith for solar minimum and maximum conditions.

Secondary particles significantly shape the lunar environment. Figure 9 shows the energy distribution of the neutron flux at the surface, where the relatively high flux reaching the detector demonstrates the importance of neutrons in lunar radiation studies. Because these secondaries carry substantial energies, they represent a serious hazard for both astronauts and electronic devices, and cannot be neglected when assessing the overall radiation environment.

The angular distributions of the neutron and gamma fluxes, shown in Figures 10 and 11, provide further insight. Both exhibit a characteristic profile: a minimum at head-on incidence ($\theta = 0°$) and a broad maximum at oblique angles, centered around $\theta \approx 70°$. This pattern arises because direct paths encounter limited mate-

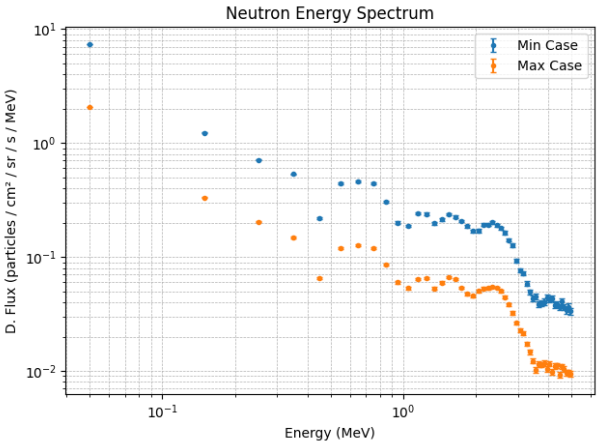

Figure 9: Neutron flux on the Moon's surface.

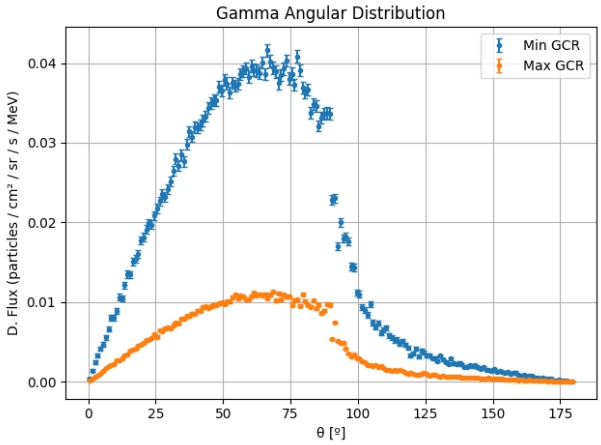

Figure 11: Angular distribution of gammas on the Moon's surface, illustrating the anisotropy of secondary particle production.

rial, while oblique trajectories traverse longer path lengths in the regolith, leading to enhanced secondary particle production through nuclear interactions. The result is a "limb-sharpened" flux that is not isotropic but strongly dependent on geometry. Although the general shape remains the same across solar minimum and maximum, the overall flux intensity is higher under solar minimum conditions, consistent with reduced solar modulation of GCRs.

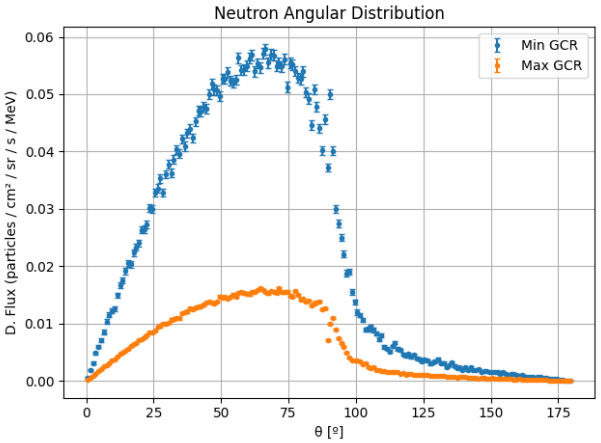

Figure 10: Angular distribution of neutrons on the Moon's surface, illustrating the anisotropy of secondary particle production.

5.5 Analysis of Linear Energy Transfer (LET)

Linear Energy Transfer (LET) is defined as the amount of energy deposited by a particle per unit path length, typically expressed in keV/μm. This quantity is crucial in radiation studies because it connects the transport of particles to their biological and material effects. High-LET particles (e.g., heavy ions, secondary neutrons) deposit energy densely along their track, producing complex DNA damage in biological tissue that is harder to repair, as well as causing single-event effects in spacecraft electronics. In contrast, low-LET radiation such as protons and electrons produces sparse ionization tracks, generally associated with lower relative biological effectiveness (RBE).

For this analysis, LET values were extracted directly from the ROOT simulation output, where each event contains information on LET in two reference media: silicon, which is a common detector material, and water, which is used as a tissue-equivalent medium. The Python analysis script processed the ROOT tree as follows:

```
n_events = tree.GetEntries()
for i in range(n_events):
tree.GetEntry(i)
hits = event.GetdMEREMHits()
totalLETWater, totalLETSi = 0.0, 0.0
for hit in hits:
totalLETWater += hit.GetLETWater()
totalLETSi    += hit.GetLETSi()
hLETWater.Fill(totalLETWater)
hLETSi.Fill(totalLETSi)
```

Figures 12a and 12b show the LET spectra in silicon and water obtained for Galactic Cosmic Rays under solar minimum conditions, across the four environments studied. The curves exhibit the typical decreasing profile: low-LET values are dominated by the abundant light primaries (mainly protons), while high-LET values correspond to rarer heavy ions and secondaries, thus appearing with much lower flux. Among the environments, the Moon exhibits the highest LET tail, reflecting the lack of shielding and the production of secondaries in the regolith. Mars presents intermediate values due to its thin atmosphere and partial shielding, while interplanetary space shows lower LET compared to the Moon because of the absence of secondaries. Earth, as expected, displays negligible LET values at the surface.

These results are consistent with the general radiation environment findings: environments without shielding (Moon, interplanetary space) are dominated by high-

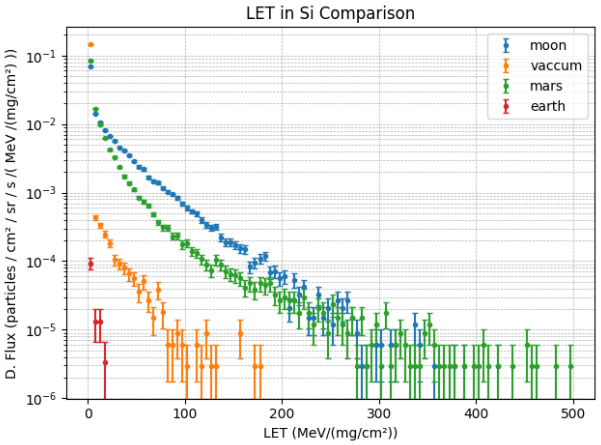

(a) Linear Energy Transfer (LET) in Silicon (Si) for all environments.

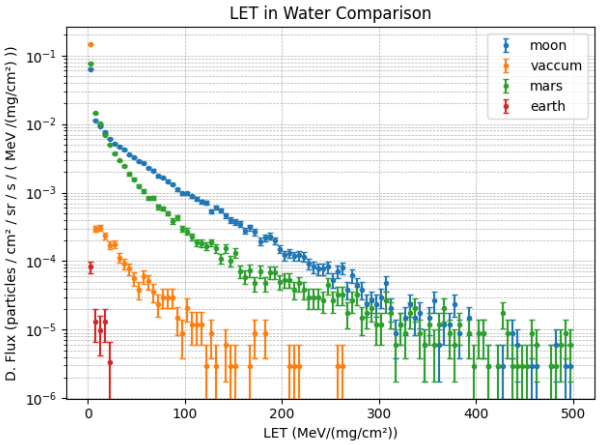

(b) Linear Energy Transfer (LET) in Water for all environments.

Figure 12: Comparison of LET in Silicon and Water across the studied environments.

LET contributions, which represent the most hazardous component for both biological and material effects.

To further validate the simulation results, they were compared with measured LET data from the Artemis I mission. Figure 13 presents LET spectra in water recorded by the HERA HSU2 instrument during the three main flight phases (inner belt, outer belt, and GCR exposure) [7]. The spectral shape is similar to that obtained in the simulations, with differences in flux normalization at low LET values, attributable to mission-specific shielding, measurement geometry and simulation constraints.

The comparison highlights the importance of LET as a metric not only for validating models but also for quantifying radiation risks in upcoming missions, particularly for the Moon, where astronauts will be exposed to the highest LET contributions among the environments studied.

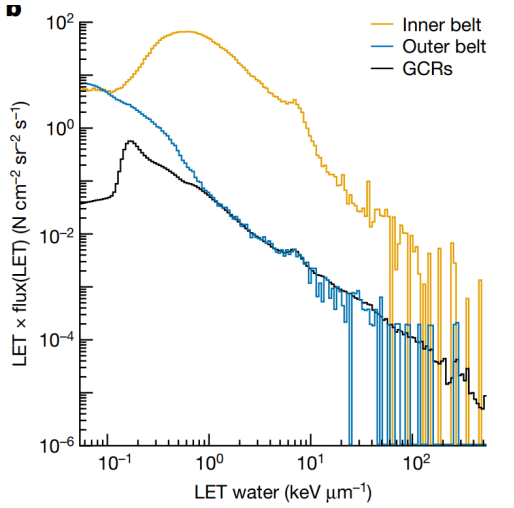

Figure 13: Measured LET spectra in water during the Artemis I mission for the inner belt, outer belt, and GCR exposure phases, as reported by the HERA HSU2 instrument.

6 Conclusions

Simulations are an extraordinary tool for space radiation studies, as they allow us to extend and generalize real data collected from missions. By combining experimental measurements with computational models, it becomes possible to explore a wide range of scenarios, particle spectra, and environments that cannot be directly accessed or replicated. This dual approach increases the reliability of our understanding and strengthens the predictive capacity of radiation transport models.

Predicting radiation levels is of the highest importance for space missions, since ionizing radiation poses risks to both astronauts and spacecraft systems. Accurate simulations are essential to guide the design of shielding materials, operational strategies, and risk mitigation protocols that ensure mission safety in challenging environments such as interplanetary space, the lunar surface, or the Martian atmosphere.

Despite the progress made, significant challenges remain. Radiation models still need refinement, particularly for environments as complex and dynamic as the Moon, where secondary particle production and interactions with the regolith introduce additional uncertainties. Improving these models will be crucial for future lunar exploration and, ultimately, for the long-duration missions to Mars and beyond.

Future Work

Future developments should focus on improving statistical precision in simulations and expanding the physics models to better describe secondary particle production, especially neutrons and gamma rays in planetary surfaces. Another key step is the systematic integration of real mission data—such as from Artemis, Mars surface missions, and

upcoming lunar orbiters—into the validation process of radiation transport codes. Finally, extending the simulations to more complex geometries and realistic shielding configurations is a critical step to move from simplified scenarios toward mission-ready risk assessment.

Acknowledgements

I would like to express my gratitude to my supervisor, Bruna Lima, whose guidance, patience, and kindness have been invaluable throughout this internship. I am also sincerely thankful to the LIP (Laboratório de Instrumentação e Física Experimental de Partículas) team for facilitating this summer internship, providing me with the opportunity to learn, explore, and deepen my understanding of such a diverse and fascinating field.

Special thanks to LIP, and particularly the SpaceRad group, for the support, and for the development of the dMEREM model and PlanetRAD, which were fundamental tools for this work. LIP is an outstanding research facility in Portugal, renowned for its contributions to experimental particle physics, and I am grateful for having had the chance to engage with its projects and expertise.

References

[1] P.C.S. Gonçalves, *The ionising radiation environment in the solar system: Sintese da lição para prestação de provas de agregação*, December 2021 (2021)

[2] R.L. Diehl, The European Physical Journal D **55**, 509 (2009)

[3] W. Hajdas, P. Gonçalves, M. Pinto, P. Socha, R. Marcinkowski, H. Xiao, F. Santos, L. Arruda, A. Galli, A. Marques et al., Space Science Reviews **221**, 43 (2025)

[4] P. Gonçalves, L. Arruda, M. Pinto, Front. Astron. Space Sci. **9**, 833144 (2022)

[5] S. McKenna-Lawlor, P. Gonçalves, A. Keating, B. Morgado, D. Heynderickx, P. Nieminen, G. Santin, P. Truscott, F. Lei, B. Foing et al., Icarus **218**, 723 (2012)

[6] S. Agostinelli et al. (GEANT4), Nucl. Instrum. Meth. A **506**, 250 (2003)

[7] S. George, R. Gaza, D. Matthiä et al., Nature **634**, 48 (2024)

[8] P.D. Group, *Review of cosmic rays*, https://pdg.lbl.gov/2021/reviews/rpp2021-rev-cosmic-rays.pdf (2021)

[9] A. Unknown, *The ionising radiation environment in the solar system*

[10] European Space Agency (ESA), *The solar cycle: a heartbeat of stellar energy*, https://www.esa.int/Science_Exploration/Space_Science/The_solar_cycle_a_heartbeat_of_stellar_energy (n.d.)

[11] B. Lima, P. Gonçalves, *The lunar ionising radiation environment: A benchmark model*, 2nd Cycle Integrated Project in Engineering Physics, Space Radiation Environment and Effects Research Group @ LIP, Portugal (2021)

[12] CERN, *Root: An object-oriented framework for large-scale data analysis*, https://root.cern (2025)

[13] SPENVIS, *Spenvis — space environment information system*, https://www.spenvis.oma.be/ (2025), accessed: 2025-09-29

Appendices

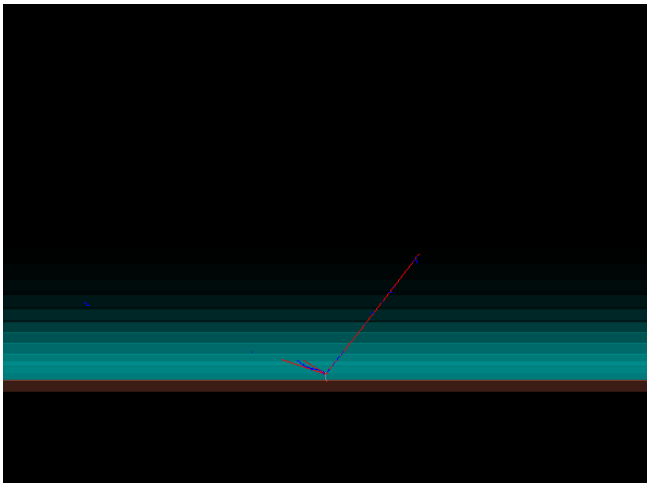

Figure 14: Visualization of a proton primary particle interacting with the Martian environment in PlanetRAD. Particle trajectories are displayed, illustrating the simulation of interactions with the atmosphere and surface.